Genetic structure of the grey side-gilled sea slug (*Pleurobranchaea maculata*) in coastal waters of New Zealand

Yeşerin Yıldırım[1*], Marti J. Anderson[1,2], Selina Patel[3], Craig D. Millar[3] and Paul B. Rainey[1,4,5]

[1]New Zealand Institute for Advanced Study, Massey University Albany, Auckland, New Zealand.

[2]Institute of Natural and Mathematical Sciences, Massey University, Auckland, New Zealand.

[3]School of Biological Sciences, University of Auckland, New Zealand

[4]Department of Microbial Population Biology, Max Planck Institute for Evolutionary Biology, Plön, Germany.

[5]Chemistry Biology Innovation (CNRS UMR 8231), Ecole supérieure de physique et de chimie industrielles de la Ville de Paris (ESPCI ParisTech), PSL Research University, Paris, France.

[*]Corresponding author

Correspondence to:
Yeşerin Yıldırım, Center for Ecology and Evolution in Microbial Systems (EEMiS), Department of Biology and Environmental Science, Linnaeus University, Kalmar, Sweden.
E-mail: yeserin.yildirim@lnu.se; **Ph:** +46 72 5949407.

Abstract

Pleurobranchaea maculata is a rarely studied species of the Heterobranchia found throughout the south and western Pacific – and recently recorded in Argentina – whose population genetic structure is unknown. Interest in the species was sparked in New Zealand following a series of dog deaths caused by ingestions of slugs containing high levels of the neurotoxin tetrodotoxin. Here we describe the genetic structure and demographic history of *P. maculata* populations from five principle locations in New Zealand based on extensive analyses of 12 microsatellite loci and the *COI* and *CytB* regions of mitochondrial DNA (mtDNA). Microsatellite data showed significant differentiation between northern and southern populations with population structure being associated with previously described regional variations in tetrodotoxin concentrations. However, mtDNA sequence data did not support such structure, revealing a star-shaped haplotype network with estimates of expansion time suggesting a population expansion in the Pleistocene era. Inclusion of publicly available mtDNA sequence from Argentinian sea slugs did not alter the star-shaped network. We interpret our data as indicative of a single founding population that fragmented following geographical changes that brought about the present day north-south divide in New Zealand waters. Lack of evidence of cryptic species supports data indicating that differences in toxicity of individuals among regions are a consequence of differences in diet.

Keywords: *Pleurobranchaea maculata*, tetrodotoxin, microsatellites, cytochrome c oxidase subunit 1, cytochrome b, population structure

Short Title: Genetic structure of *Pleurobranchaea maculata*

Introduction

The grey side-gilled sea slug *(Pleurobranchaea maculata)* is an opportunistic carnivore that feeds on invertebrates including sea anemones, marine worms and other molluscs [1]. It is native to New Zealand (NZ), southeastern Australia, China, Sri Lanka and Japan where it is found in habitats ranging from sandy sediments to rocky reefs, and from shallow sub-tidal flats to depths of 300 m [1, 2]. Little is known about the life history of the species but studies of comparative development report the production of planktotrophic veligers that hatch within eight days and remain planktonic for three weeks before juveniles settle [1-3].

In late 2009 this otherwise little-known sea slug attracted attention after it was implicated in dog deaths on beaches in Auckland [4]. Forensic analyses revealed that deaths were a consequence of tetrodotoxin (TTX) poisoning associated with ingestion of *P. maculata* [4]. This was the first time that TTX had been reported in NZ and in a species of the taxonomic clade Heterobranchia [4]. *P. maculata* that have recently invaded coastal waters of Argentina also contain TTX [5, 6].

TTX is a potent neurotoxin found in numerous terrestrial and marine organisms, but neither the origin of TTX nor the causes of variation in TTX levels among species are understood. The structure of TTX suggests a microbial origin [7] and while certain microbes have been implicated in TTX production (reviewed in Magarlamov *et al*, 2017), all such claims have been refuted [8, 9]. Nonetheless, while not excluding a microbial origin, there is recognition that TTX in animals is often acquired via diet. For example, variability in TTX levels found in puffer fish has been attributed to exposure to toxic food sources (reviewed in Noguchi and Arakawa, 2008). For *P. maculata*, there is mounting evidence that toxin accumulation occurs through feeding [10-13]. An

alternate possibility is that TTX arises from commensal or symbiotic microorganisms that are associated with *P. maculata* [13], but no TTX-producing bacteria have been found [14, 15].

Studies of individual and temporal differences in TTX concentration has established that *P. maculata* populations from northern regions of the North Island (Whangarei, Auckland, Tauranga) have high TTX concentrations (the highest average being 368.7 mg kg^{-1} per individual), while populations from the South Island (Nelson and Kaikoura) have trace amounts of TTX (<0.5 mg kg^{-1}) or none at all [2, 4, 10, 13]. A recent study reported TTX concentrations as high as 487 mg kg^{-1} [13]. Significant individual and seasonal variations have also been observed [2]. A single individual obtained from Wellington in the south of the North Island was found to have a low concentration of TTX (2.2 mg kg^{-1}) supporting the notion of a geographical cline [2].

New Zealand (NZ) extends from the subtropical Kermadec Islands (29º S) to the sub Antarctic Campbell Island group (52º S), it comprises ~700 islands affording ~15,000 km of coastline [16, 17]. Subtropical and sub-Antarctic waters converge at the juncture between the two major landmasses (the North and South Islands) creating a complex oceanography of currents and eddies.

Phylogenetic and population genetic studies of NZ marine organisms have shown that different species manifest a range of genetic structures (reviewed in Gardner *et al*, 2010) with a common pattern being a disjunction between northern and southern populations. Such disjunctions are evident in bivalves [19], teleosts [20], polyplacophores [21] , echinoderms [22] and arthropods [23].

The genetic structure of *P. maculata* is unknown, but variation in the established differences in toxicity between northern and southern populations suggests that

98 geographic variability in TTX concentration correlates genetic structure – even the
99 possibility that northern and southern populations define separate species. Here we test
100 this hypothesis using a combination of microsatellite and mitochondrial DNA (mtDNA)
101 sequence markers. Analysis of more rapidly evolving microsatellites showed evidence
102 of a genetic break along the predicted north-south divide. However, no such structure
103 was apparent from analysis of mtDNA data.

104 Materials and methods

105 Sampling, DNA extraction and tetrodotoxin assay

106 A total of 156 samples were collected from nine regions around New Zealand between
107 2009 and 2013 (Fig 1 and S1 Table). DNA was extracted as described in Yıldırım *et al*.
108 [24]. The Tauranga (TR) population included samples from Tauranga Harbour whereas
109 the Auckland (AKL) population included samples from Tamaki Strait and Waitemata
110 Harbour. Some samples were from the studies of Wood *et al*. [2] and Khor *et al*. [10].

111 **Fig 1. Sampling locations for the *Pleurobranchaea maculata* individuals.**
112 The numbers within the circles indicate the sampling size of each region. The arrows
113 show magnified maps of Auckland and Tauranga. Populations containing *P. maculata*
114 individuals with high, and low and trace amounts of tetrodotoxin concentrations in red
115 and blue colour, respectively.

116 At the outset of this study there was limited knowledge of the toxicity of *P. maculata*
117 individuals from Wellington (WL) as only one individual had been previously tested
118 [2]. To obtain a better understanding, the TTX concentration of eight (of eighteen)
119 individuals collected from WL in October 2012 was determined as described in Khor et

al. [10]. The TTX assay was performed at the Cawthron Institute (Nelson) using a liquid chromatography-mass spectrophotometry method that is described in McNabb et al. [4].

Population-level analyses were performed only for five populations which are Ti Point (TP), AKL, TR, Wellington (WL) and Nelson (NL) due to the small sample sizes of the other locations. TP, AKL and TR, which included highly toxic individuals [10] were designated as the "northern cluster", whereas the WL and NL population, which contained slightly toxic and non-toxic individuals [2, 10, 11] were designated as the "southern cluster".

Genotyping

Twelve microsatellite markers (*Pm01*, *02*, *07*, *08*, *09*, *10*, *11*, *13*, *17*, *19*, *20* and *23*) [24] were genotyped for 149 samples. PCR amplification and genotyping procedures for the primers were as described in Yıldırım *et al*. [24] with some modifications (S2 Table). Details regarding amplification and genotyping processes are described in the Supporting Information.

A 1060 bp and 1153 bp region of mitochondrial cytochrome B (*CytB*) and cytochrome oxidase I (*COI*) genes, respectively, were amplified and sequenced in all 156 *P. maculata* individuals. For details regarding the primer pairs and amplification see Supporting Information and S3 Table. Geneious Pro 6.1.6 (Biomatters, New Zealand) was used to trim, assemble, align and concatenate the resulting DNA sequences.

Statistical analysis

Genetic Diversity

Microsatellite genotyping data were tested for scoring errors due to stuttering, null alleles, and large allele dropout using MICRO-CHECKER v.2.2 [25]. Departures from

Hardy-Weinberg equilibrium (HWE) were estimated using Nei's [26] inbreeding coefficient G_{IS} with 100,000 permutations using GenoDive v2.0b25 [27]. FreeNA [28] was used to estimate null allele frequency as in Dempster *et al*. [29]. Interference of putative null alleles on genetic differentiation between sampling sites was determined by calculating global and pair-wise F_{ST} values [30], either with or without "exclusion of null alleles" [28]. Linkage disequilibrium (LD) between pairs of loci was estimated in FSTAT v2.9.3.2 [31] and the significance of LD was determined by applying a Bonferroni correction. The total number of alleles (*Na*), allele frequencies, observed heterozygosity (H_o), unbiased expected heterozygosity (H_e) corrected for a small sampling size [26], and private alleles (*PA*) per locus and population were calculated using GenAlex [32]. Allelic richness (A_R) was calculated using the rarefaction method implemented in ADZE v.1.0 [33]. H_e and A_R were used to compare the amount of genetic diversity among populations from different regions using one-way ANOVA (http://vassarstats.net).

For mtDNA, several estimates of genetic diversity, including the number of singletons (*Sin*), haplotypes (*Hap*) and segregating sites (*S*), the average number of nucleotide differences between sequences (*k*) [34], haplotype (*h*) and nucleotide diversity (π) [35] were calculated for the *CytB, COI* and concatenated sequences for each sampling location using DnaSP 5.10.0.1 [36].

Population Structure

For microsatellite data, global differentiation and pairwise differentiation between each pair of populations was investigated using various differentiation estimators, including a log-likelihood ratio (G)-based test [37], fixation index F_{ST} [30], standardised fixation index G''_{ST} [38], and Jost's [39] differentiation (*Dest*). The statistical power to detect

167 true population differentiation and α-error probability were assessed in POWSIM v4.1
168 [40]. STRUCTURE v2.3.4 [41] was used to determine the probable number of distinct
169 populations (*K*) and individuals were assigned to populations using a Bayesian
170 assignment approach. Parameters were set to 5,000,000 MCMC iterations with a burn-
171 in of 500,000 values of *K* between one and ten, with a series of ten independent
172 replicates for each *K* value, assuming an admixture model and correlated allele
173 frequencies across the populations, both with and without introducing *a priori* sampling
174 location. The most likely value of *K* was resolved using the ΔK method [42] with the
175 Structure Harvester v0.6.93 [43], and the results were introduced to the CLUMPP
176 v1.1.2 software [44]. Destruct v1.1 [45] was used to visualize the results.

177 AMOVA [46] was performed in ARLEQUIN to determine the hierarchical genetic
178 structure based on R_{ST} [47] and F_{ST} [30]for microsatellite data. Two separate
179 calculations were performed: one with structure and one without structure. For the
180 former, individuals from all regions were grouped; for the latter, the TP, AKL and TR
181 populations were grouped into a northern cluster and the WL and NL populations were
182 grouped into a southern cluster. This nested design was based on the results of
183 population structure suggested by F-statistics, multivariate and STRUCTURE analyses
184 of microsatellite data.

185 For the mtDNA sequences, POPART v1 (http://www.leigh.net.nz/software.shtml) was
186 used to create a median joining haplotype network (MJN) [48]. We created an
187 additional MJN for shorter COI sequences (624 bp) in order to accommodate four *P.*
188 *maculata* samples obtained from individuals isolated in Argentina (Farias et al., 2016).
189 A saturation test was performed in DAMBE v6.2.9 [49] using the test by Xia et al. [50].
190 The proportion of invariant sites (P_{inv}) was estimated by Jmodeltest v0.1.1 [51] with the

191 Akaike information criteria (AIC). The P_{inv} values (0.844 and 0.789 for *CytB* and *COI*,
192 respectively) obtained from the most likely models suggested by the software (HKY+I
193 and TrN+I for *CytB* and *COI*, respectively) and default settings for other parameters
194 were used for the calculations. Haplotype-frequency-based F_{ST} [26] and distance-based
195 Θ_{ST} [46] were calculated in ARLEQUIN to estimate population differentiation. For Θ_{ST},
196 the Tamura-Nei mutational model [52] was used for both genes as being the closest
197 models to the ones suggested as most likely to explain mtDNA data by Jmodeltest. For
198 concatenated sequences hierarchical structure was investigated by AMOVA in
199 ARLEQUIN using both F-statistics and Φ-statistics, and with the same structure pattern
200 used for the microsatellite data analysis (TP, AKL and TR were grouped into a northern
201 cluster, and WL and NL were grouped into a southern cluster).

202 Patterns of differentiation were also analysed using a multivariate approach. For
203 microsatellite data, the Manhattan distance (*DM*), which calculates the mean character
204 differences between individuals , and clonal distances (*DCL*), which assumes a stepwise
205 mutational model (SMM) [46], were used. For mtDNA data, a distance matrix (D_{SEQ})
206 was calculated as a standardized bp difference between every pair of individuals.
207 Statistical analyses on resulting distance matrices were done using PRIMER v6 [53]
208 with PERMANOVA+ [54]. Patterns of inter-sample distances were visualized using
209 non-metric multi-dimensional scaling ordination (MDS) [55]. Permutational
210 multivariate analysis of variance (PERMANOVA) [56, 57] was used to formally test for
211 differences in genetic structures among different locations and canonical analysis of
212 principal coordinates (CAP) [54, 58] was used to discriminate among specific
213 populations and identify their distinctiveness, using leave-one-out allocation success.
214 PERMDISP was used to test the null hypothesis of homogeneity of within-group
215 dispersions among populations [59]. All permutation tests used 10,000 permutations.

A maximum likelihood (ML) tree using the Tamura-Nei mutational model [34] with default settings was reconstructed for 44 *P. maculata* individuals from this study and three Argentinian *P. maculata* individuals using COI sequences [5] (redundant sequences were removed) in MEGA7 [60]. COI sequences of five species from the same family (Pleurobranchidae, Genbank codes in brackets) including *Pleurobranchaea meckeli* (KU365727.1), *Pleurobranchaea nevaezelandiae*, *Pleurobranchus peronii* (KM521745.1), *Berthella ocellata* (KM521694.1) and *Berthellina citrina* (KM521694.1) were used as outgroups. The analysis involved 200 informative positions of 616. The phylogeny was tested with 1,000 bootstrap replicates.

Migration

The microsatellite data were analysed with GeneClass2 [61] to identify the first-generation migrants using the Bayesian criterion of Rannala and Mountain [62] and the L_{home}/L_{max} likelihood, with a threshold *p*-value of 0.01 and a Monte-Carlo resampling algorithm [63].

Neutrality tests

BOTTLENECK v1.2 [64] was used to test the possibility of recent population reduction for microsatellite data assuming SMM and two-phase models (TPM) with default settings using a Wilcoxon signed rank test [64]. A possible sign of a recent bottleneck was investigated also by a mode-shift analysis [65].

Deviations from neutrality and demographic changes within and across the populations were calculated with Tajima's *D* [66], Fu's *Fs* [67] and mismatch distribution analysis in ARLEQUIN for the concatenated mtDNA sequences. The null hypothesis of expansion was statistically tested with the sum of squared deviations (*SSD*) from the expected values [68] and Harpending's *raggedness* index [69]. Mismatch distribution

analysis also estimated tau (τ), which is the age of the population expansion. The approximate date of population expansion across all samples was calculated for *COI* as outlined by Schenekar and Weiss [70] using http://www.unigraz.at/zoowww/mismatchcalc/index.php by converting τ to time since expansion (*t*) in years using the formula $t = \tau / 2\mu k$, where μ is the mutation rate per site per generation, and *k* is the sequence length [71]. One year of generation time and both 5.3% divergence/mya (average μ for marine invertebrate COI sequences) [72], a compatible mutation rate estimated for a planktotrophic heterobranchia species *Costasiella ocellifera* (Ellingson and Krug, 2015), were assumed. McDonald and Kreitman's [73] neutrality test was performed pooling all *P. maculata* COI sequences (1153 bp) in DnaSP using *P. meckeli* COI sequences as an outgroup species. Fisher's exact test (two-tailed) was used to identify significant deviations from neutrality.

RESULTS

Tetrodotoxin levels in P. maculata from Wellington

Previous analyses have established that northern WH, AKL, TR, and CR populations have high levels of TTX, marking these populations as "toxic", while southern populations from NL and KK are recorded as containing either trace, or no TTX [2, 4, 10, 13]. For WL populations, previous measurements existed for only one individual documented as having a low level of TTX (2.2 mg/kg) [2]. For this study, 18 slugs were obtained from WL of which eight randomly chosen individuals were subject to TTX assay. Three contained extremely low concentrations (0.12, 0.16 and 0.5 mg/kg) of TTX. No TTX was detected in the remaining five individuals. Accordingly, the WL, NL and KK samples (the southern cluster) were classified as "non-toxic".

Genetic diversity

Microsatellite analyses

All loci were highly polymorphic with between five and 23 alleles for each locus (diversity statistics in Table 1 and S4 Table). H_e across populations ranged from 0.407 to 0.843, with an average of 0.665. Rarefaction curves for A_R across each locus levelled off for each sampling location indicating that a reasonable portion of the available allelic diversity was sampled at each location (S1 Fig; allele frequencies are reported in S5 Table). Populations did not exhibit significant differences in genetic diversity for either A_R ($F_{4,146}$=0.0048, P=1.000) or H_e ($F_{4,146}$=1.102, P=0358). No significant linkage disequilibrium was found after Bonferroni correction (P<0.05) (S6 Table). Populations met Hardy-Weinberg expectations (MICROCHECKER, Table 1) with few exceptions (S4 Table). There was a low level of null allele frequency (≤ 10%) for all populations at all loci (FreeNA, S7 Table), and there were only slight changes in global and pairwise F_{ST} values between populations for each locus after accounting for null alleles (S8 Table). Original allele frequencies were therefore used in subsequent analyses.

Table 1. Summary of the genetic diversity statistics at microsatellite loci across five locations.

Locus	Na	Size (bp)	H_O	H_e	G_{IS}	F_{ST}	G''_{ST}	*Dest*
Pm01	23	108–208	0.842	0.843	0.000	0.057[c]	0.328[c]	0.291[c]
Pm02	9	105–137	0.671	0.742	0.090[a]	0.026	0.044	0.033
Pm07	10	128–164	0.737	0.720	-0.024	0.014	-0.007	-0.005
Pm08	6	141–165	0.710	0.660	-0.079	0.115[c]	0.365[c]	0.274[c]
Pm09	16	91–142	0.733	0.736	0.004	0.045[c]	0.142[c]	0.108[c]
Pm10	6	107–122	0.737	0.699	-0.055	0.071[c]	0.233[c]	0.175[c]
Pm11	11	157–187	0.838	0.813	-0.032	0.035[b]	0.137[b]	0.114[b]
Pm13	8	103–136	0.572	0.576	0.007	0.007	-0.024	-0.014

Pm17	8	155–187	0.457	0.452	-0.011	0.058[b]	0.097[b]	0.046[b]
Pm19	5	169–181	0.523	0.519	-0.008	0.041[b]	0.067[b]	0.036[b]
Pm20	5	114–132	0.407	0.407	-0.001	0.181[c]	0.340[c]	0.174[c]
Pm23	14	156–184	0.703	0.692	-0.016	0.132[c]	0.467[c]	0.378[c]
Ave	6.667		0.661	0.655	-0.009	0.064[c]	0.175[c]	0.122[c]
SE	0.428		0.020	0.019		0.014	0.046	0.0352

[a] Significant deviation from HWE (P<0.05). Significant genetic differentiation: [b] (P<0.01), [c] (P<0.001).

Mitochondrial DNA analyses

The basic diversity values for *COI* and *CytB* sequences are presented in Table 2. The total number of variable sites is 173 (*COI*: 105; *CytB*: 68), 98 of which are singleton mutations (*COI*: 59; *CytB*: 39); together these defined 130 distinct haplotypes for the concatenated sequences (*COI*: 103, *CytB*: 74). In contrast to the range of values obtained for h (0.922-0.989), the corresponding ranges for k (2.9-4.8) and π (0.254-0.414%) were low for both genes. The mean values for k and π are 7.30 (*COI*: 3.81±0.018, *CytB*: 2.75±0.018) and 0.330 % (*COI*: 0.381%, *CytB*: 0.275%), respectively for the concatenated sequences. Similar diversity was observed between sampling locations.

294 **Table 2. Summary of the genetic diversity statistics and bottleneck analysis for individuals sampled from five locations.**

		Microsatellite					*COI*						*CytB*					
Pop	***N***	***Na***	A_R	H_O	H_e	G_{IS}	***S***	***Sin***	***Hap***	***h*±SD**	***k***	**π±SD%**	***S***	***Sin***	***Hap***	***h*±SD**	***k***	**π±SD%**
Ti Point	20	6.08	6.02	0.679	0.680	0.001	27	16	17	0.984±0.020	4.8	0.414±0.048	17	9	16	0.957±0.021	3.1	0.294±0.041
Auckland	30	6.67	5.88	0.681	0.667	-0.021	39	31	26	0.989±0.013	4.1	0.352±0.033	23	15	18	0.922±0.034	2.7	0.254±0.043
Tauranga	33	6.88	5.89	0.697	0.676	-0.032	39	27	27	0.981±0.015	4.5	0.390±0.045	29	20	21	0.936±0.032	2.8	0.263±0.041
Wellington	18	6.00	6.00	0.606	0.636	0.047	25	17	16	0.987±0.023	4.2	0.363±0.033	18	10	13	0.954±0.034	3.4	0.317±0.046
Nelson	45	7.75	5.93	0.641	0.616	-0.041	44	33	30	0.957±0.018	4.0	0.348±0.035	35	23	29	0.941±0.063	2.9	0.276±0.032
Total	146	121	-	0.661	0.655	-0.009	105	59	103	0.980±0.005	4.4	0.381±0.018	68	39	74	0.945±0.011	2.9	0.275±0.018

295 *N*: sample size, *Na* number of alleles, A_R: mean allelic richness based on 18 diploid individuals, *Ho* observed heterozygosity, *He*: unbiased expected
296 heterozygosity, G_{IS}: inbreeding coefficient. *S*: number of segregating sites, *Sin*: singleton mutations, *Hap*: number of haplotypes detected, *h*: haplotype
297 diversity, *k*: number of pairwise nucleotide differences, π: nucleotide diversity, SD: standard deviation.

Genetic Structure

Microsatellite analyses

Global genetic differentiation, estimated using F_{ST}, G''_{ST} and *Dest*, was low to moderate: 0.064, 0.175 and 0.122, respectively, and highly significant ($P \leq 0.0001$). Differentiation was significant for most loci (Table 2). Location had a significant effect on population structure (PERMANOVA, *DM*: $F_{4,146}=7.3914$, *DCL*: $F_{4,146}=9.8256$, $P=0.0001$). Pairwise comparisons of genic ($\chi 2$=infinity, d.f.=24, $P<0.0001$) and genetic differentiation (F_{ST}: 0.074-0.122, G''_{ST}: 0.216-0.337, *Dest*: 0.153-0.246) as well as PERMANOVA tests (t=2.54–4.69) showed that southern populations (WL and NL) were significantly differentiated from northern populations (TP, AKL and TR) ($P<0.0001$, Table 3). Most loci supported this pairwise differentiation pattern among populations (F_{ST} and *Dest* values in S8 and S9 Tables, respectively). None of the estimators suggested significant differentiation among the northern populations of TP, AKL and TR. F_{ST} and PERMANOVA comparisons suggest weak but significant differentiation between the WL and NL populations ($P<0.046$). Analysis of statistical power by POWSIM showed a 100% probability of detecting population differentiation at an F_{ST} value of 0.01. The probability of α error was ~0.05 (P=0.04 and 0.057 based on chi-square and Fisher methods, respectively), suggesting a low risk for Type I error. The differentiation pattern was therefore considered real and reinforced by F_{ST} values between the

significantly differentiated populations being for the most part greater than 0.01. Additionally, PERMDISP analysis showed no significant differences in dispersion for either *DM* ($F_{4,141}$=0.1243, P=0.1243) or *DCL* ($F_{4,141}$= 0.4856, P=0.4856), meaning that average nucleotide distances from individuals to their own population centroid did not differ among the groups (i.e. that within-group genetic variability did not differ among populations).

Table 3. Pairwise population differentiation estimates and associated tests across five populations.

	Microsatellite data						*COI data*			*CytB data**	
Groups	**Genic**	F_{ST}	G''_{ST}	***Dest***	***t-DM***	***t-DCL***	***t***	F_{ST}	Θ_{ST}	F_{ST}	Θ_{ST}
TP-AKL	17.26	-0.009	-0.027	-0.019	0.699	0.766	1.585[a]	0.014[b]	0.024	0.050[c]	0.028
TP-TR	29.67	-0.004	-0.012	-0.008	0.727	0.79	1.359	0.017[b]	0.018	0.043[b]	0.023
TP-WL	Inf[c]	0.087[c]	0.256[c]	0.185[c]	2.851[c]	2.711[c]	1.233	0.014[a]	0.008	0.033[c]	-0.026
TP-NL	Inf[c]	0.118[c]	0.330[c]	0.241[c]	4.160[c]	4.083[c]	1.494	0.030[b]	0.029	0.040[b]	0.000
AKL-TR	20.48	-0.004	-0.011	-0.007	0.983	0.655	1.712[a]	0.015[c]	0.020	0.071[c]	0.019
AKL-WL	Inf[c]	0.095[c]	0.274[c]	0.198[c]	2.548[c]	2.958[c]	1.202	0.012[a]	0.014	0.062[c]	-0.003
AKL-NL	Inf[c]	0.122[c]	0.337[c]	0.246[c]	3.677[c]	4.693[c]	1.283	0.028[c]	0.005	0.068[c]	-0.001
TR-WL	Inf[c]	0.074[c]	0.216[c]	0.153[c]	2.541[c]	3.035[c]	1.403	0.016[a]	0.017	0.056[c]	0.012
TR-NL	Inf[c]	0.097[c]	0.272[c]	0.194[c]	3.725[c]	4.661[c]	1.076	0.031[c]	0.007	0.061[c]	0.026[a]
WL-NL	53.20[b]	0.008[a]	0.021	0.013	1.235[a]	1.593[a]	1.326	0.029[b]	0.020	0.053[c]	-0.014

$\chi 2$ values for the homogeneity of allele frequencies in pairwise comparisons tested with the exact *G*-test (Genic). Pseudo *t* statistic (*t*) from pairwise PERMANOVA tests on the basis of either Manhattan (*DM*) or Clonal distances (*DCL*) for microsatellite data, or standardized nucleotide differences for mtDNA data. Other estimators used were fixation index $F_{ST,}$ standardised fixation index $G''_{ST,}$ Jost's differentiation (*Dest*) and distance-based $\Theta_{ST.}$
TP: Ti Point, AKL: Auckland, TR: Tauranga, WL: Wellington, NL: Nelson.
Significant differentiation: [a] P<0.05, [b] P<0.0005, [c] $P\leq$0.0001. * Pairwise comparisons using pseudo t were not done for *CytB* data because the overall test was not statistically significant.

A north-south differentiation is evident from MDS ordinations of the *DM* and *DCL* matrices (Figs 2A and B). Note that although stress is relatively high (0.23 and 0.24) for the 2-dimensional MDS ordinations, the north-south distinction was also very clearly apparent in the corresponding 3-dimensional MDS ordinations (not shown here), which had lower stress (0.18 in both cases). Discriminant analysis (CAP, S2 Fig) for the two-group north-south split was highly significant ($P<0.001$), with the CAP model showing a leave-one-out allocation success of 97.26% (142/146 for *DCL* and also for *DM*). In contrast, the five-group CAP models (TP, AKL, TR, WL and NL) were poor, having overall allocation success of only 43.15% (63/146 for either *DCL* or *DM*). Furthermore, there was no discrimination among the three northern locations (TP, AKL and TR) for either *DCL* or *DM* (CAP, $P>0.76$ in both cases), justifying their pooling into a single group. Similarly, there was no basis for discriminating the two southern populations (WL and NL) using CAP models ($P > 0.11$ for *DCL* and *DM*). Bayesian clustering of individuals based on allele frequencies as implemented by STRUCTURE showed a ΔK value and mean log probabilities of data (LnP (x/K)) that were maximal at $K=2$ (Fig 2C), again supporting the same two distinct north-south clusters (Figs 2D and E). This finding was not affected by inclusion of sampling locations as priors (data not shown).

Fig 2. Visualization of genetic structure among *Pleurobranchaea maculata* populations based on microsatellite data.

All individuals from eight sampling locations were included. MDS ordination of pairwise (A) Manhattan (*DM*) and (B) Clonal (*DCL*) distances between individuals. Bayesian clustering analysis where the sampling location was not introduced for the calculations, (C) Plot of ΔK versus K indicating that data are best explained by $K = 2$ clusters, (D) Population structure at K=2. Each individual is represented by a vertical line divided into two segments, which indicates proportional membership in the two clusters; (E) Group assignments, indicating proportional membership in K=2 clusters.

AMOVA results are shown in S10 Table. Analysis performed assuming no structure revealed that the highest proportion of the total variation stemmed from variation among individuals (88.3%) with a fixation index (R_{IT}) value of 0.117. Variation between populations (R_{ST}=0.137) constituted 8.02% of the total variation with high significance (P=0.0000). Variation between individuals within populations did not contribute to genetic variation (-1.16%) (R_{IS}=-0.020, P=0.700). AMOVA analysis was repeated by clustering the populations into northern and southern clusters. The results show that the variation between the northern and southern clusters explains 20.0% (R_{CT}=0.201) of the total variation with high significance (P<0.0001). Variation between populations within clusters explained only 0.1% of the

382 total variation (R_{SC}=0.001, P=0.3418). AMOVA analysis based of F_{ST}
383 yielded similar results (data not shown). These results show that total
384 variation for the NZ *P. maculata* populations is best explained by
385 differences in the distribution of variance between northern and southern
386 clusters.

387 **Mitochondrial DNA analyses**

388 The sequence data for 156 individuals obtained from *COI* and *CytB* were
389 submitted to GenBank (accession numbers: KY094153 - KY094309 for
390 *COI* and KY094310 - KY094466 for *CytB*). MJN analysis of *CytB* (Fig 3)
391 and *COI* (S3 Fig) genes resulted in highly similar patterns. Thus, for
392 simplicity, the *CytB* network was used to infer evolutionary relationships
393 among individuals. The network shows a lack of noticeable geographical
394 structure; common haplotypes are shared across populations. The two most
395 common *CytB* haplotypes are shared by 25 (16.0% of the total dataset) and
396 22 (14.1% of the total dataset) individuals (frequencies in S11 Table). The
397 network is complex and reticulated with a star-like topology; many private
398 haplotypes descend from central shared nodes with mostly one to two base
399 pair distances [74]. Private haplotypes were detected in all sampling
400 locations. Characteristics of the network showed little change on inclusion
401 of four recently published Argentinian samples (Farias *et al*, 2015; Farias *et*
402 *al*, 2016) (based on a slightly shorter *COI* fragment (see Materials and
403 Methods and S3B Fig). Argentinian samples are closely related to NZ

404 samples with just a single base pair distance from a commonly shared
405 haplotype. The index of substitution saturation (ISS) was used to test for
406 homoplasy due to multiple substitutions [50]. For both symmetrical and
407 asymmetrical tree topology models and for both genes, the observed ISS
408 values are significantly larger than the critical *ISS* (*ISS.c*) values (S12
409 Table), which indicate that the paired partitions are not saturated, and the
410 degree of homoplasy is low.

411 **Fig 3. Median joining network of the *CytB* haplotypes.**
412 The network is coloured according to the sampling locations. The diameter
413 of the circles reflects relative haplotype frequencies. The hashes indicate the
414 mutational steps between the haplotypes. The black nodes represent the
415 imaginary haplotypes necessary to create a bridge between the present
416 haplotypes.

417 Analysis based on F_{ST} values showed a moderate but highly significant
418 global genetic differentiation for both *COI* (F_{ST}=0.022, *P*=0.0001) and *CytB*
419 (F_{ST}=0.057, *P*=0.0001). However Φ_{ST} values were significant for *COI* (Φ_{ST}
420 = 0.01552, *P* = 0.022), but not for *CytB* (Φ_{ST}=0.00845, *P*=0.12). Pairwise
421 F_{ST} values were low (0.033 – 0.074), yet significant for all the comparisons
422 (*P*< 0.03) (Table 3). Differences in the distribution of allele frequencies
423 were observable for *CytB* (Fig 4A, *COI*: S4 Fig) and pairwise Θ_{ST} values
424 were low for all the comparisons for both *COI* and *CytB* (0.007-0.029); a

weak significant differentiation was observed only between TR and NL for *CytB* (Θ_{ST}=0.026, *P*=0.0226, Table 3). MDS ordination of the D_{SEQ} matrices revealed no observable structure for either gene (Fig 4B). However, PERMANOVA analysis suggests that sampling location has a significant effect on the population structure for *COI* ($F_{4, 145}$=1.8791, *P*=0.0173), but not for *CytB* ($F_{4, 145}$=1.3386, *P*=0.1806), which was consistent with the results of Φ_{ST} analysis. Pairwise PERMANOVA tests showed significant but weak differentiation between the AKL and TP (*P*=0.0276), and AKL and TR populations (*P*=0.0218) (Table 3). PERMDISP revealed no significant differences in dispersion among populations for either *COI* ($F_{4,141}$=0.3793, *P*=0.847) or *CytB* ($F_{4, 141}$=0.358, *P*=0.833). CAP analysis was performed for *COI* but not for *CytB* because PERMANOVA did not reveal significant differences between groups for the latter. A CAP analysis to discriminate the three northern populations was statistically significant (trace=0.293, *P*=0.0038, S5 Fig), but the populations varied in their degree of distinctiveness under the CAP model. Specifically, leave-one-out cross-validation had the highest allocation success for TR (69.7%), followed by AKL (50%), but there was little or no identifiability of samples from Ti Point (only 25% correct allocation). Overall, the CAP results were consistent with the structures revealed by PERMANOVA: among the five populations, AKL is weakly distant from TP and TR.

Fig 4. Graphical visualization of the results of population structure and demographic analysis for mtDNA data.

(A) The frequencies of *CytB* haplotypes at each location (*N*=156). The pie segment represents the relative haplotype frequencies. Each colour corresponds to a different haplotype. The patterned segment represents private haplotypes. The sizes of the circles are proportional to the sample size. (B) Non-metric MDS ordination of distances obtained from the standard nucleotide differences between individuals for the *COI* data. Each symbol also represents a different sampling location.(C) Mismatch distributions of pairwise base pair differences between the concatenated *COI* and *CytB* haplotypes.

PERMANOVA analysis was repeated by contrasting the TP, AKL and TR populations (the northern population cluster) against WL and NL (the southern population cluster) to test whether the north-south differentiation identified with microsatellite data could be observed with the mtDNA data. The results indicate no significant differentiation between the clusters (*COI*: $F_{1, 145}$=0.819, *P*=0.5268; *CytB*: $F_{1, 145}$=1.2325, *P*=0.2982) and do not support the north-south differentiation identified by microsatellite data.

Hierarchical AMOVA analysis of concatenated sequences performed in the absence of population structure showed that differentiation among sampling sites explains only 0.69% and 1.26% of the total variation based on Θ_{ST} and

467 F_{ST} statistics, respectively, with high significance (Θ_{ST}=0.01260,
468 P=0.03082; F_{ST}=0.00686, P=0.0001), whereas variation within populations
469 explained 98.74% (Θ_{ST}) or 99.31% (F_{ST}) of the total variation (S13 Table).
470 Grouping of populations into northern and southern clusters explained a
471 maximum 0.16% of the total variation, but it was not significant (Θ_{CT}=-
472 0.0062, P=0.8994; F_{CT} = 0.00161, P=0.10029). These analyses show that
473 mtDNA data do not support the north-south differentiation evident in
474 microsatellite data.

475 A phylogenetic analysis of *P. maculata* shows that *P. maculata* samples
476 from NZ form a single clade (S6 Fig). Inclusion of the Argentinian
477 sequences did not change the topology of the tree. Phylogenetic
478 relationships between *P. maculata* individuals were unsupported (bootstrap
479 values <50%), whereas there was good bootstrap support (between 74-
480 100%) for five other species in the Pleurobranchidae family.

481 # Migration and demographic changes

482 ## Microsatellite analyses

483 Migration analysis with GeneClass2 detected four first generation migrants
484 (P=0.01): one individual sampled from TP is a migrant from AKL, one
485 individual sampled from TR is from AKL, and two individuals sampled
486 from NL are migrants from WL (S14 Table). Individuals from each cluster
487 were more likely to belong to populations from the same cluster. A lack of

first generation migrants between the clusters shows that these clusters are genetically not well connected. However, CAP and STRUCTURE show low connectivity between the clusters and admixed individuals in both northern and southern clusters (Figs 2D and E). The highest misclassifications between the clusters detected by CAP analysis and highest admixture proportions detected by STRUCTURE were noted in TR and WL. This suggests that the TR and WL populations are bridges between the clusters. Admixture in the WL population may also explain weak differentiation between the WL and NL populations that was found with F_{ST} and PERMANOVA tests.

The Wilcoxon test did not detect recent bottlenecks in any population under either TPM or SMM models (Table 4). In addition, analysis of mode-shift in the distribution of allele frequencies suggests that all the populations exhibit a normal L-shaped pattern indicating no mode-shift in the frequency distribution of alleles. Taken together these data suggest that none of the populations experienced a recent or sudden bottleneck.

Table 4. Results of the neutrality and demographic tests using either microsatellite or mtDNA data.

	Microsatellite		mtDNA – concatenated sequences				
	Bottleneck					Mismatch Distribution	
Population	TPM	SMM	Tajima's *D*	Fu's *Fs*	τ	*SSD* (P_{SSD})	*Raggedness* (P_r)
Ti Point	0.741	0.945	-1.45	-14.57[c]	8.783	0.010 (0.368)	0.033 (0.184)
Auckland	0.715	0.993	-2.14[b]	-23.57[c]	5.254	0.017 (0.028)	0.008 (0.980)
Tauranga	0.689	0.995	-2.10[b]	-24.93[c]	7.590	0.001 (0.873)	0.006 (0.968)
Wellington	0.633	0.052	-1.62[a]	-9.47[c]	7.691	0.001 (0.944)	0.011 (0.852)

Nelson	0.954	0.999	-2.20[b]	-25.08[c]	7.994	0.001 (0.870)	0.006 (0.953)
Total	-	-	-2.45[c]	-24.74[c]	7.797	0.001 (0.756)	0.004 (0.929)

Total values for Tajima's *D*, Fu's *Fs*, τ and the parameters of the mismatch distribution analysis were calculated pooling all available individuals into a single pool.
TPM: Two-phase mutational model, SMM: stepwise mutational model, *SSD*: sum of squared deviations and statistical significance, P_{SSD}: for the validity of the sudden expansion model, τ: time passed since population expansion, r*aggedness* and P_r*:* Harpending's raggedness index and its probability' respectively, for the null hypothesis test of goodness-of-fit. *P*-values: [a] <0.05, [b] <0.01, [c] <0.001

Mitochondrial DNA analyses

Overall, neutrality tests of Tajima's *D* and Fu's *Fs* revealed significant negative values in pooled samples (Table 4) suggesting a recent population expansion or purifying selection. This was also suggested by the uni-modal mismatch distributions of pairwise base pair differences for *COI* and *CytB* haplotypes (Fig 4Cand S7 Fig, respectively), non-significant *SSD* and *raggedness* patterns (Table 4). Furthermore, the McDonald-Kreitman test found no evidence of positive selection: the ratio of nonsynonymous to synonymous substitutions within *P. maculata* (*Pn/Ps*=5/136) and between species (*Dn/Ds*=5/100) was statistically similar (neutrality index=0.400, *P*=0.1104).

The demographic parameter tau (τ), which represents the mutational time since expansion, was calculated after pooling all five populations (pooling of populations was justified because all exhibited signs of population expansion): τ was estimated at 2.703 (CI 95%: 1.488-3.320) and 2.754 (CI 95%: 1.344-3.615) for the *COI* and *CytB* data, respectively. The date of

expansion was estimated at 44.2 kya (CI 95%: 24.3-54.3 kya) based on *COI* data.

DISCUSSION

This study marks the first attempt to describe and account for patterns of genetic diversity in *P. maculata*. Overall, we observed marked signals of population structure; however, the population structure suggested by microsatellite versus mtDNA data differed. The nuclear data exhibit patterns of diversity indicative of a north-south disjunction. The northern samples formed one group and southern (WL and NL) samples formed another (with few examples of migration). However this disjunction was not supported by F_{ST} analysis of mtDNA data, which indicated divergence among all populations.

Discordance between results obtained from nuclear versus mitochondrial markers is not uncommon, with explanations ranging from variation in lineage sorting to differences in rates of nuclear versus mitochondrial evolution [reviewed in 75, 76]. Taken together, we interpret our data as indicative of a single founding population that subsequently became fragmented following geographical and oceanographical changes that led to the present north-south divide in NZ waters.

550 According to this scenario, *P. maculata* was inhabiting the NZ waters
551 before the end of the last glacial maximum when sea levels were low and
552 NZ was a single land mass [77, 78]. Shallow-water species that inhabit
553 intertidal or shallow subtidal areas were primarily affected as decreased sea
554 levels destroyed available habitat [79, 80]. At some later time, most likely
555 following the last glacial maximum (~22,000 years ago), large benthic
556 habitats became available [79], and this may have facilitated population
557 expansion and fragmentation aided by warming temperatures and rising sea
558 levels [81].

559 In support of this model is the haplotype network based on mtDNA data
560 showing star-like structure and high haplotype diversity, indicative of a
561 population expansion arising from a small initial population [74]. Additional
562 support comes from the unimodal mismatch distribution pattern of pairwise
563 base pair differences for *COI* and *CytB* haplotypes (Fig 4C and S6 Fig,
564 respectively), non-significant *SSD* and *raggedness* patterns (Table 4), and
565 significant negative values for Tajima's *D* and Fu's *Fs*. The approximate
566 date of population expansion was estimated at 44.2 kya (CI: 24.3–54.3kya).
567 This estimate assumes a 5.3% divergence rate for the COI gene, which
568 while an estimate, nonetheless coincides with a periodic of cyclic climatic
569 oscillation defined by the late Pleistocene era (~110–15 kya) [82].
570 Glaciation has been suggested as the possible cause of demographic changes

571 in other NZ marine organisms, including triplefin species [20] and red alga
572 *Bostrychia intricata* [83].

573 This scenario is also supported by the analysis of more rapidly evolving
574 microsatellites, which are useful for uncovering recent barriers to gene flow
575 [84-86], especially following periods of demographic expansion [84, 86].
576 As sea levels rose at the end of the last glacial cycle [~13,000 years ago;
577 78], geographical factors and associated oceanography established barriers
578 to gene flow for marine organisms. In particular, confluence of the East
579 Cape current with the Wairarapa Eddy off the east coast of the North Island
580 (between 37–39°S) created an oceanographic barrier [87]. A barrier was
581 also formed by waters separating North and South Islands (the Cook Strait)
582 [87, 88].

583 A north-south genetic differentiation has been observed in other marine
584 organisms from NZ (reviewed in Gardner et al, 2010; Ross et al, 2012).
585 Confluence of the East Cape current with the Wairarapa Eddy is thought to
586 be responsible for population differentiation in organisms such as the
587 amphipods *Paracorophium excavatum* and *P. lucasi* [87] and the gastropod
588 *Diloma subrostrata* [89]. The Cook Strait barrier is thought to have
589 underpinned north-south differentiation in organisms such as the green shell
590 mussel (*Perna canaliculus*) [19], blackfoot paua (*Haliotis iris*) [21] and the
591 Ornate limpet (*Cellana ornate*) [90].

592 One additional factor that has likely promoted recent population subdivision
593 in *P. maculata* is the distribution of invasive species [91] that constitute a
594 food source for *P. maculata*. The Asian date mussel, *Arcuatula senhousia*
595 has been established in the Auckland region since the 1970s, forming large
596 transient beds in sub- and inter-tidal areas of the Hauraki Gulf, Manukau
597 Harbour and Whangarei Harbour [92]. Expansion of *A. senhousia* beds in
598 the Hauraki Gulf appears to have preceded increases in the density of *P.*
599 *maculata* populations. Interestingly, subsequent decline of near-shore beds
600 of *A. senhousia* post 2010 was followed by rapid decline in the density of *P.*
601 *maculata* populations [93]. Further evidence that range expansion of *P.*
602 *maculata* may have been facilitated by availability of prey species comes
603 from off-shore mussel farms in Tasman Bay (Nelson, NZ), where culture of
604 the green shell and blue mussels have created new habitats for *P. maculata*,
605 with high-density populations being found beneath mussel farms [93].
606 Recently, *P. maculata* was identified in Argentinean waters with the species
607 rapidly spreading along the Atlantic coast [5, 6]. The minor difference
608 between mtDNA sequence in Argentinian versus NZ raises the possibility
609 that NZ maybe the source of the recently discovered Argentinian
610 population.

611 Life history traits such as the nature of egg and larval stages are of
612 understandable importance in shaping population structure of the species.
613 Species with benthic eggs tend to have more structured populations than

ones with pelagic eggs [94, 95] and an inverse relationship between pelagic larval duration (PLD) and genetic structure has been found [96, 97]: in a comparative analysis of NZ pelagic marine species, Ross et al. [96] showed a significant negative correlation between PLD and genetic differentiation. However, in the same meta-study, when NZ-wide sampling regimes were considered, NZ organisms with PLD durations similar to *P. maculata* (2–4 weeks) exhibit structural patterns of diverse types ranging from no structure, to a north-south disjunction, IBD and differentiation within and between sampling locations [96].

Our prediction that the previously recorded cline in TTX might be explained by genetic structure holds only for microsatellite markers. Had this also held for mtDNA markers a case may have been made that *P. maculata* is a complex of two cryptic species, but no such evidence exists. Our phylogenetic analysis indicates that all *P. maculata* populations – including samples from Argentinian waters [5] – are conspecific. Short branches with no or low bootstrap support is also indicative of lack of genetic differentiation among *P. maculata*. Similar lack of differentiation between toxic and non-toxic populations has been shown for *Taricha granulosa* newts from various localities in western North America [98, 99] and the red-spotted newt *Notophthalmus viridescens* [100].

Having called into question substantive genetic differences between north and south populations, differences in TTX levels are thus likely attributable to exogenous factors, such as differences in associated bacteria, exposure, or diet. Work to date is strongly suggestive of diet as the major source of TTX, with *P. maculata* accumulating TTX via feeding [10], while offspring from TTX positive individuals raised in a TTX-free environment become free of TTX [12]. Recent work studying cultured bacteria from *P. maculata* found no evidence for a bacterial origin of the toxin [15], but TTX has been reported in certain prey, including a Platyhelminthes *Stylochoplana* species, that co-occur with TTX-containing *P. maculata* [11].

ACKNOWLEDGEMENTS

We acknowledge Susanna Wood and David Taylor (Cawthron Institute); Lauren Salvitti, Dudley Bell and Warrick Powrie (The University of Waikato); Mike McMurtry (Auckland Regional Council); Severine Hannam and Wilma Blom (Auckland Museum); Shane Genage (Victoria University of Wellington); Steve Journee (The Dive Guys, Wellington); Richard Huges, Paul Caiger and Bakhti Patel (The Leigh Marine Laboratory at the University of Auckland); and Don Morrisey, Matthew Smiths and Stephen Brown (The National Institute of Water and Atmospheric Research). We thank Paul McNabb (Cawthron Institute) and Serena Khor (The University of Waikato) for conducting tetrodotoxin assays.

Supporting Information accompanies this paper on the website.

REFERENCES

1. Willan R. New-Zealand side-gilled sea slugs (Opisthobranchia, Notaspidea, Pleurobranchidae). Malacologia. 1983;23(2):221-70.

2. Wood SA, Taylor DI, McNabb P, Walker J, Adamson J, Cary SC. Tetrodotoxin concentrations in *Pleurobranchaea maculata*: temporal, spatial and individual variability from New Zealand populations. Mar Drugs. 2012;10(1):163-76.

3. Gibson GD. Larval development and metamorphosis in *Pleurobranchaea maculata*, with a review of development in the Notaspidea (Opisthobranchia). Bio Bull. 2003;205(2):121-32.

4. McNabb P, Selwood AI, Munday R, Wood SA, Taylor DI, Mackenzie LA, et al. Detection of tetrodotoxin from the grey side-gilled sea slug - Pleurobranchaea maculata, and associated dog neurotoxicosis on beaches adjacent to the Hauraki Gulf, Auckland, New Zealand. Toxicon. 2010;56(3):466-73.

5. Farias N, Wood S, Obenat S, Schwindt E. Genetic barcoding confirms the presence of the neurotoxic sea slug *Pleurobranchaea maculata* in southwestern Atlantic coast. N Z J Zool. 2016;43(3):292-8.

675 6. Farias NE, Obenat S, Goya AB. Outbreak of a neurotoxic side-gilled
676 sea slug (*Pleurobranchaea* sp.) in Argentinian coasts. N Z J Zool.
677 2015;42(1):51-6.
678 7. Noguchi T, Arakawa O. Tetrodotoxin - Distribution and
679 accumulation in aquatic organisms, and cases of human intoxication.
680 Mar Drugs. 2008;6(2):220-42.
681 8. Magarlamov TY, Melnikova DI, Chernyshev AV. Tetrodotoxin-
682 Producing Bacteria: Detection, Distribution and Migration of the
683 Toxin in Aquatic Systems. Toxins. 2017;9(5).
684 9. Matsumura K. Reexamination of Tetrodotoxin Production by
685 Bacteria. Appl Environ Microb. 1995;61(9):3468-70.
686 10. Khor S, Wood SA, Salvitti L, Taylor DI, Adamson J, McNabb P, et
687 al. Investigating diet as the source of tetrodotoxin in
688 *Pleurobranchaea maculata*. Mar Drugs. 2014;12(1):1-16.
689 11. Salvitti L, Wood SA, Taylor DI, McNabb P, Cary SC. First
690 identification of tetrodotoxin (TTX) in the flatworm *Stylochoplana*
691 sp.; a source of TTX for the sea slug *Pleurobranchaea maculata*.
692 Toxicon. 2015;95:23-9.
693 12. Wood SA, Casas M, Taylor DI, McNabb P, Salvitti L, Ogilvie S, et
694 al. Depuration of tetrodotoxin and changes in bacterial communities
695 in *Pleurobranchea maculata* adults and egg masses maintained in
696 captivity. J Chem Ecol. 2012;38(11):1342-50.

13. Salvitti L, Wood SA, Fairweather R, Culliford D, McNabb P, Cary SC. In situ accumulation of tetrodotoxin in non-toxic *Pleurobranchaea maculata* (Opisthobranchia). Aquat Sci. 2017;79(2):335-44.

14. Chau R, Kalaitzis JA, Wood SA, Neilan BA. Diversity and biosynthetic potential of culturable microbes associated with toxic marine animals. Mar Drugs. 2013;11(8):2695-712.

15. Salvitti LR, Wood SA, McNabb P, Cary SC. No evidence for a culturable bacterial tetrodotoxin producer in *Pleurobranchaea maculata* (Gastropoda: Pleurobranchidae) and *Stylochoplana* sp. (Platyhelminthes: Polycladida). Toxins (Basel). 2015;7(2):255-73.

16. West CJ, Thompson AM. Small, dynamic and recently settled: responding to the impacts of plant invasions in the New Zealand (Aotearoa) archipelago. In: Foxcroft LC, Pysek P, Richardson DM, Genovesi P, editors. Plant Invasions in Protected Areas: Patterns, Problems and Challenges. Dordrecht.: Springer; 2013. p. 285-311.

17. Wallis GP, Trewick SA. New Zealand phylogeography: evolution on a small continent. Mol Ecol. 2009;18(17):3548-80.

18. Gardner J, Bell J, Constable H, Hannan D, Ritchie P, Zuccarello G. Multi-species coastal marine connectivity: a literature review with recommendations for further research. N Z Aquat Environ Biodiversity Rep. 2010;58:1-47.

719 19. Wei KJ, Wood AR, Gardner JPA. Population genetic variation in the
720 New Zealand greenshell mussel: locus-dependent conflicting signals
721 of weak structure and high gene flow balanced against pronounced
722 structure and high self-recruitment. Mar Biol. 2013;160(4):931-49.
723 20. Hickey AJ, Lavery SD, Hannan DA, Baker CS, Clements KD. New
724 Zealand triplefin fishes (family Tripterygiidae): contrasting
725 population structure and mtDNA diversity within a marine species
726 flock. Mol Ecol. 2009;18(4):680-96.
727 21. Waters JM, King TM, O'Loughlin PM, Spencer HG.
728 Phylogeographical disjunction in abundant high-dispersal littoral
729 gastropods. Mol Ecol. 2005;14(9):2789-802.
730 22. Ayers KL, Waters JM. Marine biogeographic disjunction in central
731 New Zealand. Mar Biol. 2005;147(4):1045-52.
732 23. Schnabel KE, Hogg ID, Chapman MA. Population genetic structures
733 of two New Zealand corophiid amphipods and the presence of
734 morphologically cryptic species: implications for the conservation of
735 diversity. New Zeal J Mar Fresh. 2000;34(4):637-44.
736 24. Yıldırım Y, Patel S, Millar CD, Rainey PB. Microsatellite
737 development for a tetrodotoxin-containing sea slug
738 (*Pleurobranchaea maculata*). Biochem Syst Ecol. 2014;55:342-5.
739 25. Van Oosterhout C, Hutchinson WF, Wills DP, Shipley P.
740 MICRO-CHECKER: software for identifying and correcting

741 genotyping errors in microsatellite data. Mol Ecol Notes.
742 2004;4(3):535-8.
743 26. Nei M. Estimation of average heterozygosity and genetic distance
744 from a small number of individuals. Genetics. 1978;89(3):583-90.
745 27. Meirmans PG, Van Tienderen PH. GENOTYPE and GENODIVE:
746 two programs for the analysis of genetic diversity of asexual
747 organisms. Mol Ecol Notes. 2004;4(4):792-4.
748 28. Chapuis M-P, Estoup A. Microsatellite null alleles and estimation of
749 population differentiation. Mol Biol Evol. 2007;24(3):621-31.
750 29. Dempster AP, Laird NM, Rubin DB. Maximum likelihood from
751 incomplete data via the EM algorithm. J R Stat Soc Ser B (Method).
752 1977;39(1):1-38.
753 30. Weir BS, Cockerham CC. Estimating F-statistics for the analysis of
754 population structure. Evolution. 1984:1358-70.
755 31. Goudet J. FSTAT (Version 1.2): A computer program to calculate F-
756 statistics. J Hered. 1995;86(6):485-6.
757 32. Peakall R, Smouse PE. GENALEX 6: genetic analysis in Excel.
758 Population genetic software for teaching and research. Mol Ecol
759 Notes. 2006;6(1):288-95.
760 33. Kalinowski ST. hp-rare 1.0: a computer program for performing
761 rarefaction on measures of allelic richness. Mol Ecol Notes.
762 2005;5(1):187-9.

763 34. Tajima F. Evolutionary relationship of DNA sequences in finite
764 populations. Genetics. 1983;105(2):437-60.
765 35. Nei M. Molecular Evolutionary Genetics. New York: Columbia
766 University Press; 1987.
767 36. Librado P, Rozas J. DnaSP v5: a software for comprehensive
768 analysis of DNA polymorphism data. Bioinformatics.
769 2009;25(11):1451-2.
770 37. Raymond M, Rousset F. An exact test for population differentiation.
771 Evolution. 1995;49(6):1280-3.
772 38. Hedrick PW. A standardized genetic differentiation measure.
773 Evolution. 2005;59(8):1633-8.
774 39. Jost L. GST and its relatives do not measure differentiation. Mol
775 Ecol. 2008;17(18):4015-26.
776 40. Ryman N, Palm S. POWSIM: a computer program for assessing
777 statistical power when testing for genetic differentiation. Mol Ecol
778 Notes. 2006;6(3):600-2.
779 41. Pritchard JK, Stephens M, Donnelly P. Inference of population
780 structure using multilocus genotype data. Genetics.
781 2000;155(2):945-59.
782 42. Evanno G, Regnaut S, Goudet J. Detecting the number of clusters of
783 individuals using the software STRUCTURE: a simulation study.
784 Mol Ecol. 2005;14(8):2611-20.

785 43. Earl DA. STRUCTURE HARVESTER: a website and program for
786 visualizing STRUCTURE output and implementing the Evanno
787 method. Conserv Genet Resour. 2012;4(2):359-61.
788 44. Jakobsson M, Rosenberg NA. CLUMPP: a cluster matching and
789 permutation program for dealing with label switching and
790 multimodality in analysis of population structure. Bioinformatics.
791 2007;23(14):1801-6.
792 45. Rosenberg NA. DISTRUCT: a program for the graphical display of
793 population structure. Mol Ecol Notes. 2004;4(1):137-8.
794 46. Excoffier L, Smouse PE, Quattro JM. Analysis of molecular
795 variance inferred from metric distances among DNA haplotypes:
796 application to human mitochondrial DNA restriction data. Genetics.
797 1992;131(2):479-91.
798 47. Slatkin M. A measure of population subdivision based on
799 microsatellite allele frequencies. Genetics. 1995;139(3):1463-.
800 48. Bandelt HJ, Forster P, Röhl A. Median-joining networks for
801 inferring intraspecific phylogenies. Mol Biol Evol. 1999;16(1):37-
802 48.
803 49. Xia X. DAMBE5: a comprehensive software package for data
804 analysis in molecular biology and evolution. Mol Biol Evol.
805 2013;30(7):1720-8.

806 50. Xia X, Xie Z, Salemi M, Chen L, Wang Y. An index of substitution
807 saturation and its application. Mol Phylogenet Evol. 2003;26(1):1-7.
808 51. Posada D. jModelTest: Phylogenetic Model Averaging. Mol Biol
809 Evol. 2008;25(7):1253-6.
810 52. Tamura K, Nei M. Estimation of the number of nucleotide
811 substitutions in the control region of mitochondrial DNA in humans
812 and chimpanzees. Mol Biol Evol. 1993;10(3):512-26.
813 53. Clarke K, Gorley R. PRIMER v6: User Manual/Tutorial: PRIMER-
814 E Ltd: Plymouth, UK; 2006.
815 54. Anderson MJ, Gorley RN, Clarke KR. PERMANOVA+ for
816 PRIMER: Guide to Software and Statistical Methods: PRIMER-E:
817 Plymouth, UK; 2008.
818 55. Kruskal JB. Nonmetric multidimensional scaling: a numerical
819 method. Psychometrika. 1964;29(2):115-29.
820 56. Anderson MJ. A new method for non-parametric multivariate
821 analysis of variance. Austral Ecol. 2001;26(1):32-46.
822 57. McArdle BH, Anderson MJ. Fitting multivariate models to
823 community data: a comment on distance-based redundancy analysis.
824 Ecology. 2001;82(1):290-7.
825 58. Anderson MJ, Willis TJ. Canonical analysis of principal coordinates:
826 a useful method of constrained ordination for ecology. Ecology.
827 2003;84(2):511-25.

828 59. Anderson MJ. Distance-based tests for homogeneity of multivariate
829 dispersions. Biometrics. 2006;62(1):245-53.
830 60. Kumar S, Stecher G, Tamura K. MEGA7: Molecular Evolutionary
831 Genetics Analysis Version 7.0 for Bigger Datasets. Mol Biol Evol.
832 2016;33(7):1870-4.
833 61. Piry S, Alapetite A, Cornuet J-M, Paetkau D, Baudouin L, Estoup A.
834 GENECLASS2: a software for genetic assignment and first-
835 generation migrant detection. J Hered. 2004;95(6):536-9.
836 62. Rannala B, Mountain JL. Detecting immigration by using multilocus
837 genotypes. Proc Natl Acad Sci U S A. 1997;94(17):9197-201.
838 63. Paetkau D, Slade R, Burden M, Estoup A. Genetic assignment
839 methods for the direct, real-time estimation of migration rate: a
840 simulation-based exploration of accuracy and power. Mol Ecol.
841 2004;13(1):55-65.
842 64. Piry S, Luikart G, Cornuet JM. BOTTLENECK: a computer
843 program for detecting recent reductions in the effective size using
844 allele frequency data. J Hered. 1999;90(4):502-3.
845 65. Luikart G, Cornuet JM. Empirical evaluation of a test for identifying
846 recently bottlenecked populations from allele frequency data.
847 Conserv Biol. 1998;12(1):228-37.
848 66. Tajima F. Statistical method for testing the neutral mutation
849 hypothesis by DNA polymorphism. Genetics. 1989;123(3):585-95.

850 67. Fu Y-X. Statistical tests of neutrality of mutations against population
851 growth, hitchhiking and background selection. Genetics.
852 1997;147(2):915-25.
853 68. Schneider S, Excoffier L. Estimation of past demographic
854 parameters from the distribution of pairwise differences when the
855 mutation rates vary among sites: application to human mitochondrial
856 DNA. Genetics. 1999;152(3):1079-89.
857 69. Harpending H. Signature of ancient population growth in a low-
858 resolution mitochondrial DNA mismatch distribution. Hum Biol.
859 1994:591-600.
860 70. Schenekar T, Weiss S. High rate of calculation errors in mismatch
861 distribution analysis results in numerous false inferences of
862 biological importance. Heredity. 2011;107(6):511.
863 71. Liao P-C, Kuo D-C, Lin C-C, Ho K-C, Lin T-P, Hwang S-Y.
864 Historical spatial range expansion and a very recent bottleneck of
865 *Cinnamomum kanehirae* Hay.(Lauraceae) in Taiwan inferred from
866 nuclear genes. BMC Evol Biol. 2010;10(1):124.
867 72. Crandall ED, Sbrocco EJ, DeBoer TS, Barber PH, Carpenter KE.
868 Expansion dating: calibrating molecular clocks in marine species
869 from expansions onto the Sunda Shelf following the Last Glacial
870 Maximum. Mol Biol and Evol. 2011;29(2):707-19.

871 73. McDonald JH, Kreitman M. Adaptive protein evolution at the Adh
872 locus in Drosophila. Nature. 1991;351(6328):652.
873 74. Slatkin M, Hudson RR. Pairwise comparisons of mitochondrial
874 DNA sequences in stable and exponentially growing populations.
875 Genetics. 1991;129(2):555-62.
876 75. Toews DP, Brelsford A. The biogeography of mitochondrial and
877 nuclear discordance in animals. Mol Ecol. 2012;21(16):3907-30.
878 76. Zink RM, Barrowclough GF. Mitochondrial DNA under siege in
879 avian phylogeography. Mol Ecol. 2008;17(9):2107-21.
880 77. Lewis KB, Carter L, Davey FJ. The opening of Cook Strait:
881 interglacial tidal scour and aligning basins at a subduction to
882 transform plate edge. Mar Geol. 1994;116(3-4):293-312.
883 78. Trewick S, Bland K. Fire and slice: palaeogeography for
884 biogeography at New Zealand's North Island/South Island juncture. J
885 R Soc N Z. 2012;42(3):153-83.
886 79. Allcock AL, Strugnell JM. Southern Ocean diversity: new
887 paradigms from molecular ecology. Trends Ecol Evol.
888 2012;27(9):520-8.
889 80. Norris RD, Hull PM. The temporal dimension of marine speciation.
890 Evol Ecol. 2012;26(2):393-415.

81. Weaver PP, Carter L, Neil HL. Response of surface water masses and circulation to late Quaternary climate change east of New Zealand. Paleoceanography. 1998;13(1):70-83.

82. Gradstein FM, Ogg JG, Smith AG, Bleeker W, Lourens LJ. A new geologic time scale, with special reference to Precambrian and Neogene. Episodes. 2004;27(2):83-100.

83. Muangmai N, Fraser CI, Zuccarello GC. Contrasting patterns of population structure and demographic history in cryptic species of Bostrychia intricata (Rhodomelaceae, Rhodophyta) from New Zealand. J Phycol. 2015;51(3):574-85.

84. Barr KR, Lindsay DL, Athrey G, Lance RF, Hayden TJ, Tweddale SA, et al. Population structure in an endangered songbird: maintenance of genetic differentiation despite high vagility and significant population recovery. Mol Ecol. 2008;17(16):3628-39.

85. Edwards S, Bensch S. Looking forwards or looking backwards in avian phylogeography? A comment on. Mol Ecol. 2009;18(14):2930-3.

86. Zink RM, Groth JG, Vázquez-Miranda H, Barrowclough GF. Phylogeography of the California Gnatcatcher (*Polioptila californica*) using multilocus DNA sequences and ecological niche modeling: Implications for conservation. The Auk. 2013;130(3):449-58.

913 87. Stevens MI, Hogg ID. Population genetic structure of New Zealand's
914 endemic corophiid amphipods: evidence for allopatric speciation.
915 Biol J Linnean Soc. 2004;81(1):119-33.
916 88. Keeney DB, Szymaniak AD, Poulin R. Complex genetic patterns
917 and a phylogeographic disjunction among New Zealand mud snails
918 *Zeacumantus subcarinatus* and *Z. lutulentus*. Mar Biol.
919 2013;160(6):1477-88.
920 89. Donald KM, Kennedy M, Spencer HG. Cladogenesis as the result of
921 long-distance rafting events in South Pacific topshells (Gastropoda,
922 Trochidae). Evolution. 2005;59(8):1701-11.
923 90. Goldstien SJ, Schiel DR, Gemmell NJ. Comparative
924 phylogeography of coastal limpets across a marine disjunction in
925 New Zealand. Mol Ecol. 2006;15(11):3259-68.
926 91. Rodriguez LF. Can invasive species facilitate native species?
927 Evidence of how, when, and why these impacts occur. Biol
928 Invasions. 2006;8(4):927-39.
929 92. Crooks JA. Characterizing ecosystem-level consequences of
930 biological invasions: the role of ecosystem engineers. Oikos.
931 2002;97(2):153-66.
932 93. Taylor DI, Wood SA, McNabb P, Ogilvie S, Cornelisen C, Walker J,
933 et al. Facilitation effects of invasive and farmed bivalves on native

populations of the sea slug Pleurobranchaea maculata. Mar Ecol Prog Ser. 2015;537:39-48.

94. Riginos C, Douglas KE, Jin Y, Shanahan DF, Treml EA. Effects of geography and life history traits on genetic differentiation in benthic marine fishes. Ecography. 2011;34(4):566-75.

95. Riginos C, Buckley YM, Blomberg SP, Treml EA. Dispersal Capacity Predicts Both Population Genetic Structure and Species Richness in Reef Fishes. Am Nat. 2014;184(1):52-64.

96. Ross PM, Hogg ID, Pilditch CA, Lundquist CJ. Phylogeography of New Zealand's coastal benthos. N Z J Mar Freshwater Res. 2009;43(5):1009-27.

97. Selkoe KA, Toonen RJ. Marine connectivity: a new look at pelagic larval duration and genetic metrics of dispersal. Mar Ecol Prog Ser. 2011;436:291-305.

98. Hanifin CT, Brodie Jr ED, Brodie III ED. Phenotypic mismatches reveal escape from arms-race coevolution. PLoS Biol. 2008;6(3):e60.

99. Ridenhour BJ, Brodie Jr ED, Brodie III ED. Patterns of genetic differentiation in *Thamnophis* and *Taricha* from the Pacific Northwest. J Biogeogr. 2007;34(4):724-35.

100. Yotsu-Yamashita M, Gilhen J, Russell RW, Krysko KL, Melaun C, Kurz A, et al. Variability of tetrodotoxin and of its analogues in the

red-spotted newt, *Notophthalmus viridescens* (Amphibia: Urodela: Salamandridae). Toxicon. 2012;59(2):257-64.

Supporting Information Captions

Supporting Information Text: Supplementary Methodology and Results

S1 Table. Sampling locations and abbreviations for the New Zealand *Pleurobranchaea maculata* populations.

S2 Table. PCR annealing temperature and elongation time for microsatellite markers.

S1 Table. Primers used to amplify the mtDNA genes.

S2 Table. Summary genetic diversity statistics for the 12 microsatellites and 5 populations of *Pleurobranchaea maculata*.

S3 Table. Allele frequencies at 12 microsatellite loci by population.

S4 Table. Results of the linkage equilibrium test for 12 microsatellite markers. The calculations were performed for each population and across the populations. *P* values were estimated by 6600 permutations. The *P*-value for the 5% nominal level is 0.000152 after Bonferroni correction.

S5 Table. Estimating the null allele frequency using the ENA algorithm.

974 **S6 Table. The estimation of the possible effect of null alleles on**
975 **population structure analysis.** Estimated (A) global F_{ST} of Weir (1996) for
976 each microsatellite locus and (B) pairwise F_{ST} for each pair of populations
977 with and without using the ENA correction [28].

978 **S9 Table. Pairwise population matrix of the *Dest* values at each locus.**
979 ***Dest* values below the diagonal.** The *P* values calculated with 9999
980 permutations are shown above the diagonal. TP: Ti Point, AKL: Auckland,
981 TR: Tauranga, WL: Wellington, NL: Nelson.

982 **S10 Table. AMOVA results for the *Pleurobranchaea maculata***
983 **populations based on the microsatellite data.** Analysis was performed
984 with SMM based on R_{ST}-statistics. The hierarchical distribution of variation
985 was determined between the sampling locations without introducing any
986 structure, and nesting the Ti Point-Auckland and Tauranga populations in
987 the northern cluster and the Wellington and Nelson populations in the
988 southern cluster.

989 **S3 Fig. Median joining network of the *COI* haplotypes.** (A) 1153 bp of
990 *COI* sequences from 156 New Zealand individuals. (B) 624 bp of *COI*
991 sequences from 156 New Zealand and four Argentinian individuals. The
992 network was coloured according to the sampling locations. The diameters of
993 the circles are proportional to the frequency of the haplotypes. The hashes
994 indicate the mutational steps between the haplotypes. The black nodes

represent the imaginary haplotypes necessary to create a bridge between the present haplotypes.

S11 Table. Haplotype frequencies for the mtDNA sequences by mere counting in populations. The IDs are individual names. [+]Population codes. *Sample size.

S12 Table. The results of the saturation test for *COI* and C*ytB* sequences. The results suggest only little saturation both genes while assuming both symmetrical and asymmetrical topology as significant difference was observed between *Iss* and *Iss*.c values, and *Iss* < *Iss*.*c*.

S13 Table. AMOVA results of concatenated *COI* and *CytB* sequences based on F- and Θ-statistics.

S14 Table. Detection of first generation migrants. Likelihood ratio: L_home/L_max. The number of individuals with a probability below the threshold value is 4. The potential migrants are labelled in red ($P < 0.01$) and the most likely population in green. ID: ID of the individuals.

S1 Fig. Allele rarefaction curves for the microsatellite data.

S2 Fig. CAP analyses of the multivariate genetic distances between the *P. maculata* individuals obtained from 12 microsatellite markers. (A) *DM* (the number of axes - *m*=13) and (B) *DCL* (*m*=6) distances. The axes

represent the amount of variation between the populations that is explained by the two axes. Each symbol represents a different sampling location.

S3 Fig. Median joining network of the *COI* haplotypes. (A) 1153 bp of *COI* sequences from 156 New Zealand individuals. (B) 624 bp of *COI* sequences from 156 New Zealand and four Argentinian individuals. The network was coloured according to the sampling locations. The diameters of the circles are proportional to the frequency of the haplotypes. The hashes indicate the mutational steps between the haplotypes. The black nodes represent the imaginary haplotypes necessary to create a bridge between the present haplotypes.

S4 Fig. The graphical representation of haplotypes frequencies for *COI* data at each sampling location. The pie segment represents the relative frequencies of the haplotypes. Each colour corresponds to a different haplotype. Private haplotypes specific to each location are represented with a patterned segment.

S5 Fig. Graphical visualization of the standard nucleotide differences between individuals based on the *COI* data. Canonical correlation ordination analysis at m=4 was performed.

S6 Fig. Molecular phylogenetic analysis of COI sequences by maximum likelihood method. The tree with the highest log likelihood (-2685.86 is displayed. Initial tree(s) for the heuristic search were obtained automatically

by applying Neighbor-Join and BioNJ algorithms to a matrix of pairwise distances estimated using the Maximum Composite Likelihood (MCL) approach, and then selecting the topology with superior log likelihood value. The analysis involved 49 nucleotide sequences out of a total of 616. The nodes are coloured based on the sampling locations. The numbers on the nodes represent the % bootstrap support (values <50% not presented).

S7 Fig. Mismatch distribution of pairwise base pair differences between the concatenated *COI* and *CytB* haplotypes.

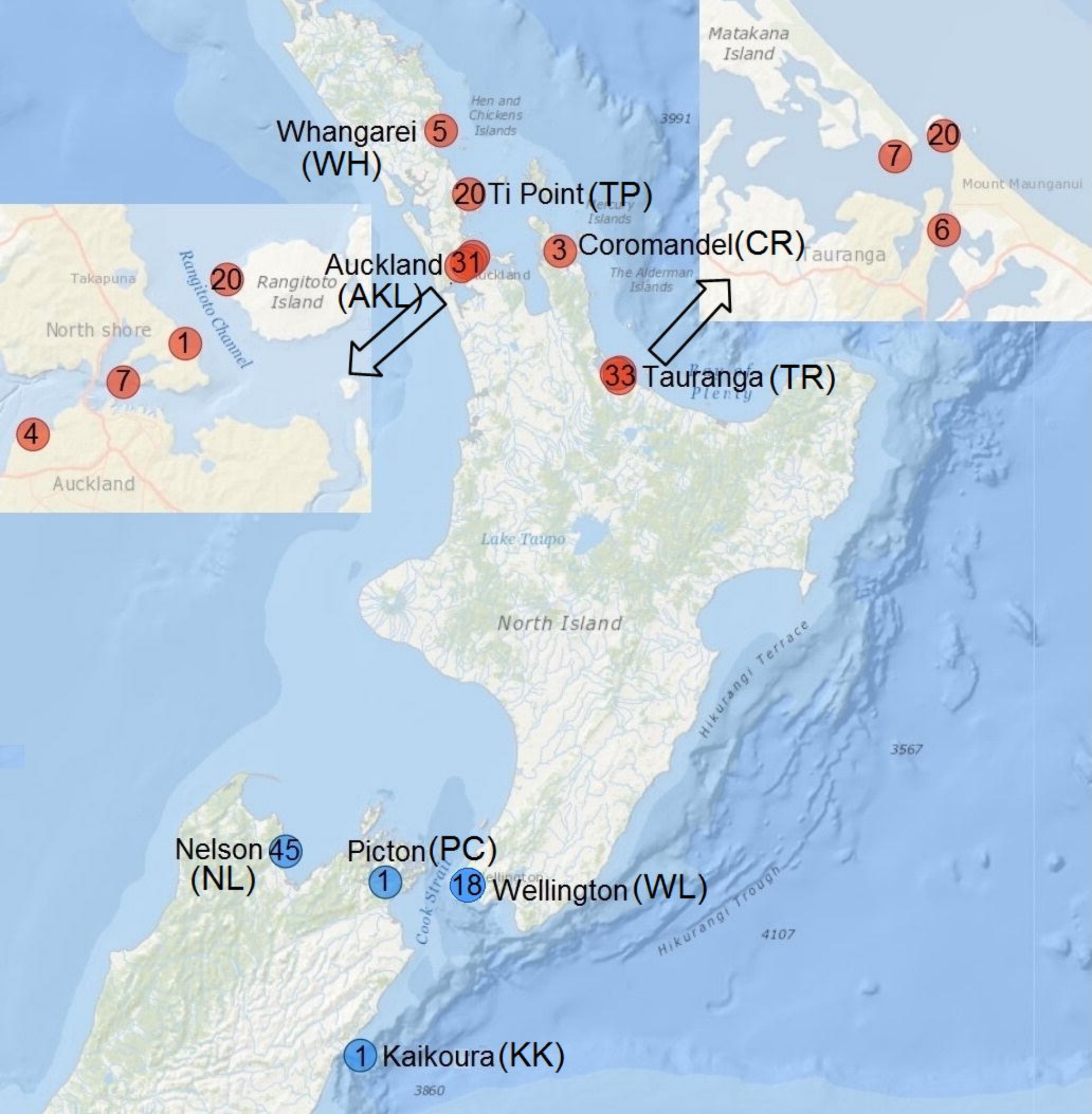
Whangarei (WH)
5
20 Ti Point (TP)
3 Coromandel (CR)
Auckland (AKL)
31
33 Tauranga (TR)
Nelson (NL)
45
Picton (PC)
1
18 Wellington (WL)
1 Kaikoura (KK)
20
7
6
1
7
4
Matakana Island
Hen and Chickens Islands
3991
Mount Maunganui
Tauranga
Takapuna
Rangitoto Island
Rangitoto Channel
North shore
Auckland
The Alderman Islands
Lake Taupo
North Island
Hikurangi Terrace
3567
Hikurangi Trough
4107
Cook Strait
3860

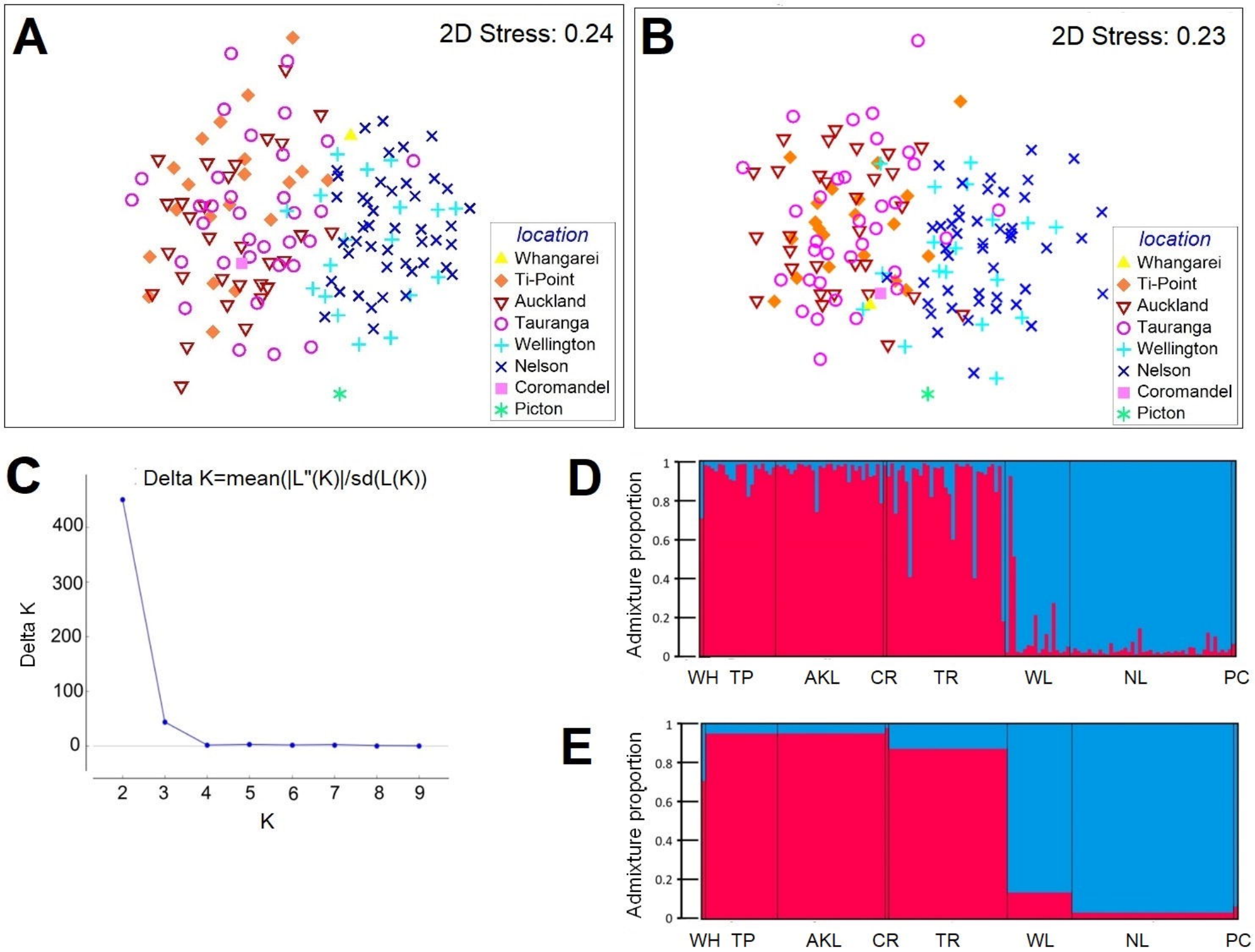
A
2D Stress: 0.24
location
Whangarei
Ti-Point
Auckland
Tauranga
Wellington
Nelson
Coromandel
Picton
B
2D Stress: 0.23
location
Whangarei
Ti-Point
Auckland
Tauranga
Wellington
Nelson
Coromandel
Picton
C
Delta K=mean(|L"(K)|/sd(L(K))
Delta K
400
300
200
100
0
2
3
4
5
6
7
8
9
K
D
Admixture proportion
1
0.8
0.6
0.4
0.2
0
WH
TP
AKL
CR
TR
WL
NL
PC
E
Admixture proportion
1
0.8
0.6
0.4
0.2
0
WH
TP
AKL
CR
TR
WL
NL
PC

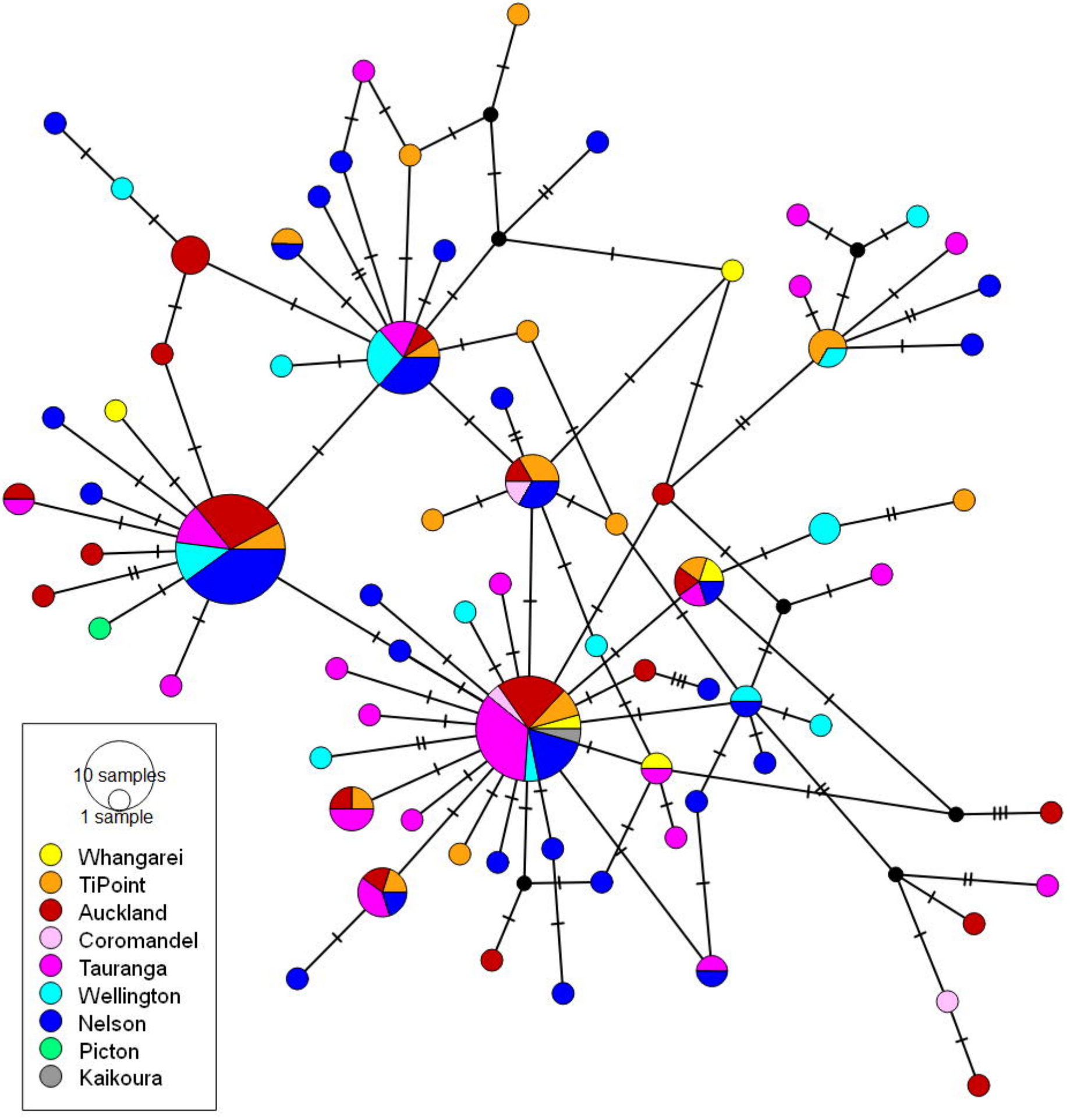
10 samples
1 sample
Whangarei
TiPoint
Auckland
Coromandel
Tauranga
Wellington
Nelson
Picton
Kaikoura

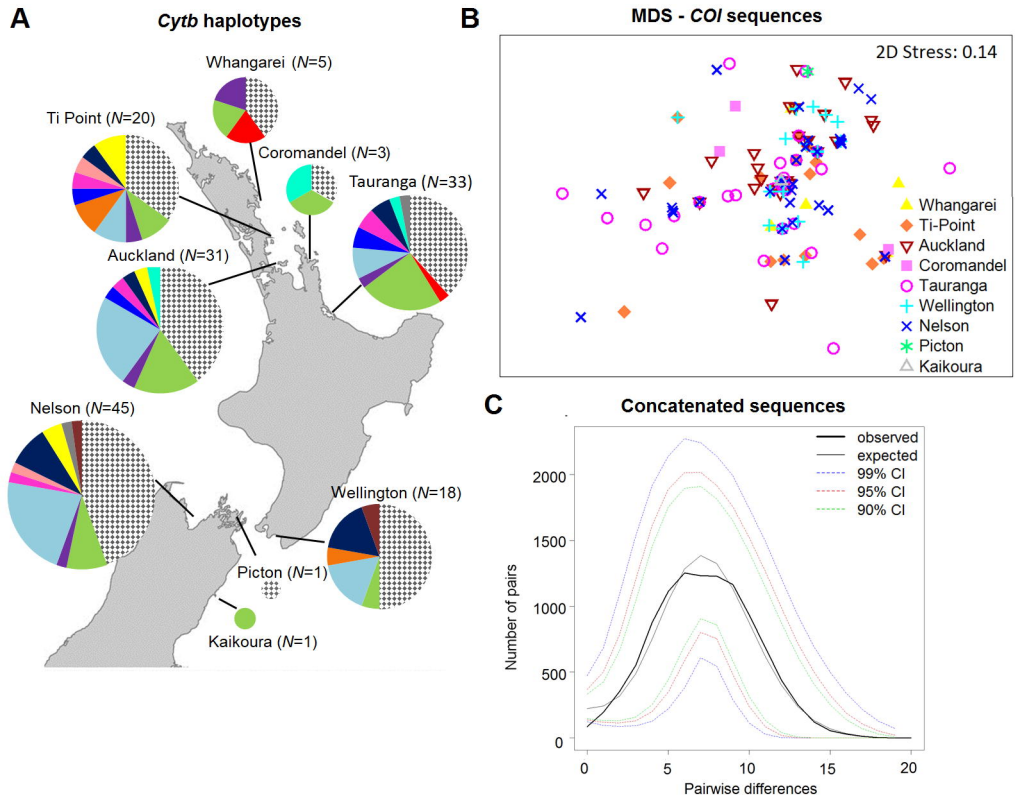
A
Cytb haplotypes
Whangarei (N=5)
Ti Point (N=20)
Coromandel (N=3)
Tauranga (N=33)
Auckland (N=31)
Nelson (N=45)
Wellington (N=18)
Picton (N=1)
Kaikoura (N=1)
B
MDS - COI sequences
2D Stress: 0.14
Whangarei
Ti-Point
Auckland
Coromandel
Tauranga
Wellington
Nelson
Picton
Kaikoura
C
Concatenated sequences
observed
expected
99% CI
95% CI
90% CI
Number of pairs
0
500
1000
1500
2000
0
5
10
15
20
Pairwise differences